X-625-72-18

PREPRINT



# EVIDENCE FOR THE EXISTENCE OF NEGATIVE IONS IN THE D- AND LOWER E- REGIONS AT TWILIGHT

J. A. KANE

FEBRUARY 1972

GSFC — GODDARD SPACE FLIGHT CENTER

GREENBELT, MARYLAND

X-625-72-18

# EVIDENCE FOR THE EXISTENCE OF NEGATIVE IONS IN THE D- AND LOWER E-REGIONS AT TWILIGHT

J. A. Kane

February 1972

GODDARD SPACE FLIGHT CENTER
Greenbelt, Maryland

# EVIDENCE FOR THE EXISTENCE OF NEGATIVE IONS IN THE D- AND LOWER E-REGIONS AT TWILIGHT

by

J. A. Kane

Laboratory for Planetary Atmospheres

NASA-Goddard Space Flight Center

Greenbelt, Maryland

## ABSTRACT

Our evidence for negative ions in the lower ionosphere is based on the difference between simultaneously measured profiles of electron and positive ion density. The electron density profiles reported here were obtained from ground-to-rocket radio wave absorption measurements while Gerdien ion traps were used to measure the positive ion profiles. Results from a series of three rockets launched from Thumba, India near sunset on 27 March, 1970 indicate that a significant number of negative ions are formed at altitudes as high as 95 km at twilight.

# EVIDENCE FOR THE EXISTENCE OF NEGATIVE IONS IN THE D- AND LOWER E-REGIONS AT TWILIGHT

## 1. INTRODUCTION

In the past few years our knowledge of the lower ionosphere has increased remarkably. The various sources of ion production have been identified and for the most part fairly well evaluated as to relative importance. In situ ion identification combined with laboratory measurements of various ion chemistry rate coefficients have begun to clarify the major loss processes for positive ions. However, our present picture of the lower ionosphere suffers from a conspicuous blind spot in the electron production and loss process, namely the role played by negative ions. The existence of negative ions in the lowermost regions of the ionosphere can be inferred from the ion mobility measurements of Hale et al. (1968). More recently, direct sampling of ionospheric negative ion composition (Narcisi et al., 1971; Arnold et al., 1971) has revealed a wide spectrum of negative ion mass numbers to be present in the D- and lower E-regions. However, direct measurement of the absolute value of the negative ion density does not appear to be practical at the present time. It is likely that this quantity can be obtained more easily as the difference between simultaneously measured values of the electron and positive ion density.

This report is concerned primarily with our attempts to deduce negative ion densities by comparing radio propagation measurements of electron density profiles with simultaneous probe measurements of positive ion densities. A secondary objective of this report is to present a series of electron density profiles for a latitude and range of solar zenith angles for which relatively little has been reported, namely the equatorial ionosphere during twilight.

The electron density in the lower ionosphere is fairly well known at middle latitudes. This is due to the efforts of numerous workers using various radio techniques both ground based and rocket borne. By comparison, the lower ionosphere at equatorial latitudes has not received much attention. This is unfortunate since from a theoretical stand point equatorial measurements should be of prime interest. Long term radio wave absorption studies by Gnanalingam (1969) indicate that the anomolous day to day variability so characteristic of the mid-latitude winter mesosphere seems to be either absent or at least greatly reduced at the equator. It is well established that mesospheric air pressures, densities and temperatures undergo significant variations, both day to day as well as seasonal. The magnitudes of both these variations however are smallest at lowest latitudes. This meteorological stability together with the presumed absence of energetic particle precipitation removes from the equatorial D-region two of the most unpredictable variables of the mid-latitude D-region. The equator is therefore the ideal place from which to study the build up and decay of a D-region which is under a simple solar zenith angle control.

In this report we present the results of D- and E-region electron and positive ion density measurements obtained from ARCAS rockets launched at Thumba, India in March 1970. Also included are the results of a previous campaign at Thumba in March 1968 at which time only electron densities were measured.

The electron densities reported here were deduced from absorption measurements on ground-to-rocket radio transmissions propagating transversely to the earth's magnetic field. The technique and results of the radio experiments are described in part 2. The simultaneous positive ion measurements were obtained by means of rocket borne Gerdien ion traps. The theory and performance of this

trap is the subject matter of part 3 of this report. The Gerdien's major sources of error, namely shock wave and vehicle potential effects, are treated in some detail in Appendices A-1 and A-2. Finally in part 4 we give our conclusions and recommendations concerning the efficacy of similar experiments in the future.

## 2. ELECTRON DENSITIES

### 2.1 Method of Measurement

One of the reasons why equatorial D-region electron densities have received little experimental attention is the fact that the radio techniques employed in rocket experiments at mid-latitudes become inappropriate near the magnetic equator. Mid-latitude radio techniques are all based on the so called quasi-longitudinal or Q.L. approximation to the Appleton-Hartree formula. Near the magnetic equator the Q.L. approximation breaks down for the radio frequencies (2-3 MHz) required for D-region measurements. However at the magnetic equator (within $\pm 1$ or 2 degrees) it is possible with a vertically propagating radio wave to satisfy the conditions of the other extreme of the Appleton-Hartree formula, namely the quasi-transverse or Q.T. approximation.

A unique experimental advantage accrues to the Q.T. condition, namely the fact that the two characteristic waves are linearly polarized. To transmit either mode one simply radiates from a horizontal linear dipole antenna oriented parallel (ordinary mode) or perpendicular (extraordinary mode) to the magnetic meridian. Compare this with the mid-latitude case where the transmission of a characteristic mode requires a pair of crossed dipoles combined in a precise phase and amplitude relationship. In the Q.T. regime there occurs no Faraday rotation (in the normal meaning of the term).. However absorption is operative on either mode and the absorption indicies are related to the electron density and

collision frequency in a straightforward manner. This was the basis of the following experimental technique.

On the ground the output of a 100 watt CW transmitter was alternately switched between a north-south (ordinary) and an east-west (extraordinary) half wave dipole antenna. See Goddard Document X-615-69-499 (Kane, 1969) for details of the switching technique. In the rocket the amplitude of the arriving wave was sampled at a 30 cycle/sec rate by a linearly polarized receiving antenna, the sampling frequency being twice the rocket spin frequency. In addition to a pre-flight calibration of the receiver input-output characteristic, an in-flight calibration was obtained by manually stepping the transmitter output through 30 db of attenuation in 6 db steps.

A sample of the telemetry flight record is shown in Figure 1. Here is seen the amplitude of the received signal strengths of two CW transmissions at 2115 and 1865 kHz as the ordinary and extraordinary modes are alternately transmitted from the ground. Differential absorption is clearly visible. A plot of absorption observed for both modes is shown versus altitude in Figure 2 for a transmission frequency of 1865 kHz.

2.2 Data Reduction

Trajectory determinations on our 1968 Thumba rockets were accurate to approximately ±1 km. A significant improvement was obtained on our 1970 Thumba rockets with a slant range tracking system (Hudgins and Lease, 1969) which yielded trajectories accurate to ±50 meters.

From the altitude derivative of the absorption on either polarization mode, the electron density profile was deduced by means of the Generalized Appleton-Hartree formula (see for example Sen and Wyller, 1960). The model collision

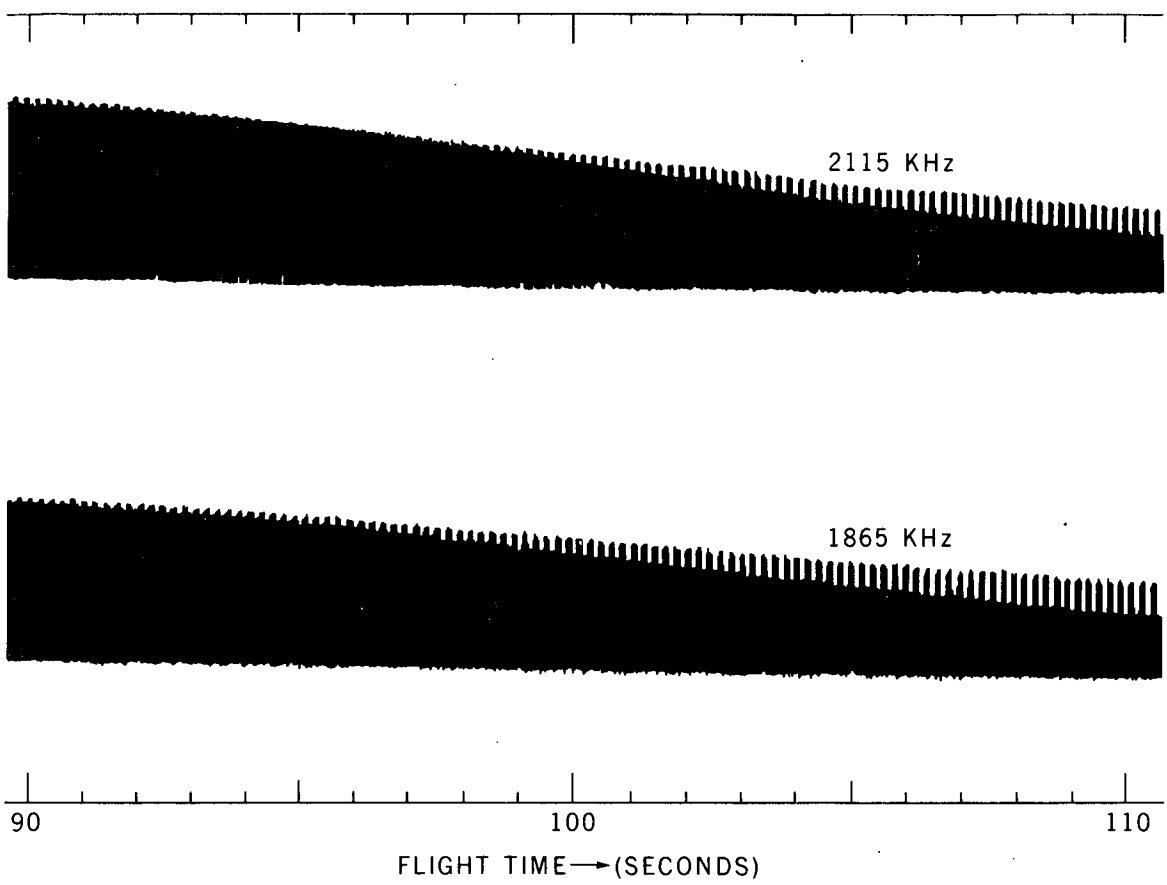


Figure 1. Sample of telemetry record showing signal strength received at rocket as ground based transmitter is alternately switched between ordinary and extraordinary polarization modes.

frequency profile given in Tables I and II was assumed. This model was taken from the pressure measurements made at 0° latitude, 8 March 1965 (Smith et al., 1967) together with the expression of Phelps (1960)

$$\nu = 6.20 \times 10^5 \, p \text{ (MKS)} \qquad (2.2:1)$$

relating the collision frequency $\nu$ to atmospheric pressure p given in MKS units. By performing the absorption measurements on more than one frequency, the requirement of internal consistency provides a check on the appropriateness of the choice of collision frequency model.

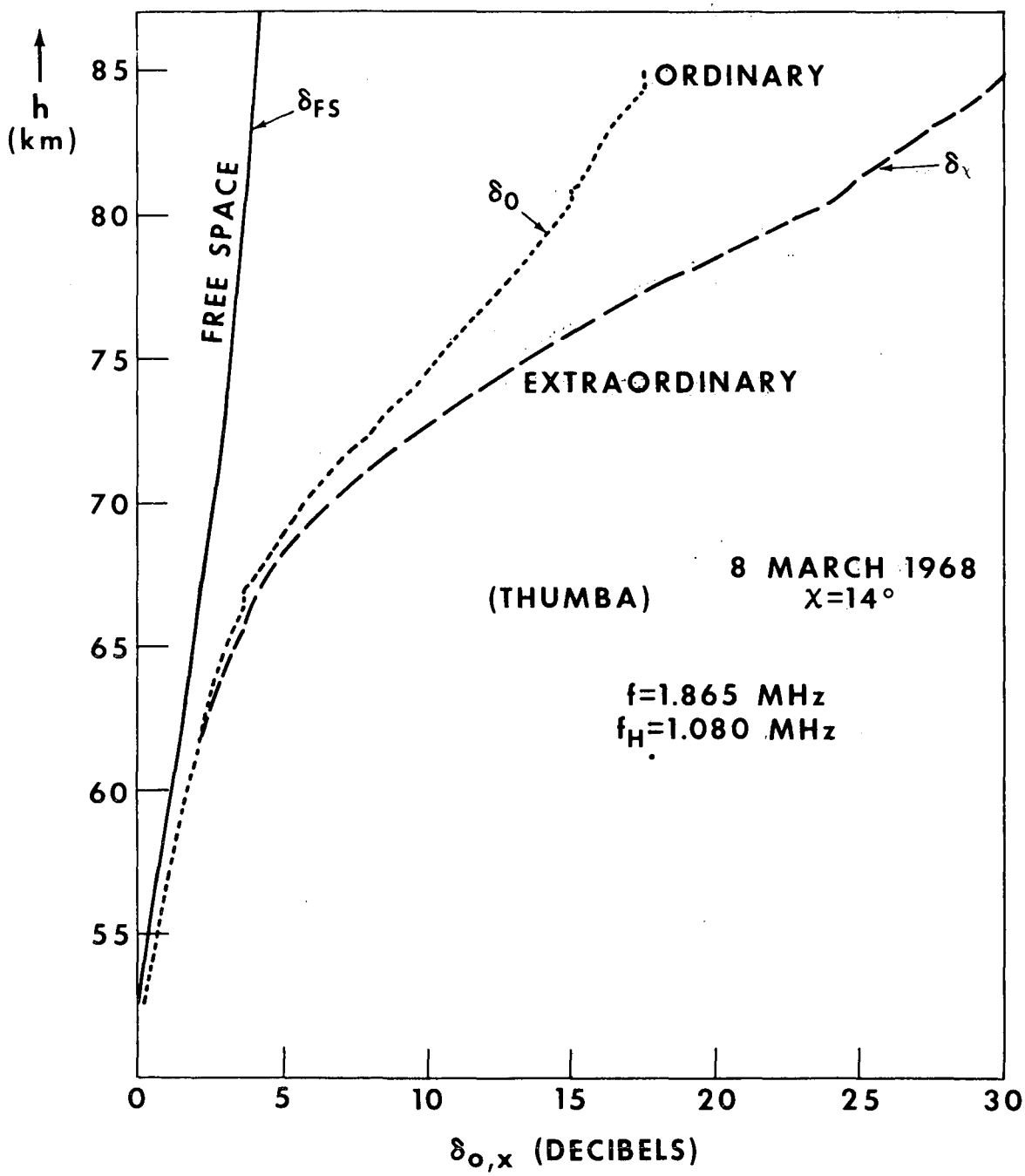


Figure 2. Absorption versus altitude for both polarization modes measured at transmission frequency f = 1.865 MHz. The local gyro-frequency at 85 km is $f_H$ = 1.080 MHz.

TABLE I

| h (km) | $\nu$ ($sec^{-1}$) | Mar '70 $\chi = 6°$ N ($cm^{-3}$) | Mar '68 $\chi = 14°$ N ($cm^{-3}$) |
|---|---|---|---|
| 84 | $4.10^5$ | | $2.3^3 \pm 5.0^2$ |
| 82 | 5.80 | | $1.0^3 \pm 2.0^2$ |
| 80 | 8.10 | | $1.0^3 \pm 2.0^2$ |
| 78 | $1.12^6$ | | $1.0^3 \pm 2.0^2$ |
| 76 | 1.55 | | $7.9^2 \pm 1.5^2$ |
| 74 | 2.15 | | $6.3^2 \pm 1.5^2$ |
| 72 | 3.00 | | $6.0^2 \pm 1.5^2$ |
| 70 | 4.10 | | $3.8^2 \pm 1.0^2$ |
| 68 | 5.60 | $6.0^2 \pm 1.5^2$ | $2.5^2 \pm 1.0^2$ |
| 66 | 7.50 | $3.0^2 \pm 1.0^2$ | $1.6^2 \pm 7.5^1$ |
| 64 | $1.00^7$ | $2.0^2 \pm 5.0^1$ | $1.3^2 \pm 7.5^1$ |
| 62 | 1.30 | $1.0^2 \pm 5.0^1$ | $1.0^2 \pm 5.0^1$ |
| 60 | 1.70 | $9.0^1 \pm 5.0^1$ | $7.5^1 \pm 5.0^1$ |
| 57 | 2.45 | $9.0^1 \pm 5.0^1$ | |
| 54 | 3.60 | $9.0^1 \pm 5.0^1$ | |
| 51 | 5.10 | $1.2^2 \pm 5.0^1$ | |

## 2.3 Electron Density Results

The results of our electron density measurements at Thumba are given in Tables I and II. As might be expected if meteorological and energetic particle effects are negligible in the equatorial mesosphere, the electron density profile obtained at $\chi = 86°$ in 1970 is similar to the 1968 profile measured at the

TABLE II

| h (km) | $\nu$ (sec$^{-1}$) | Mar '70 $\chi$ = 98° N (cm$^{-3}$) | Mar '70 $\chi$ = 92° N (cm$^{-3}$) | Mar '70 $\chi$ = 86° N (cm$^{-3}$) | Mar '68 $\chi$ = 86° N (cm$^{-3}$) |
|---|---|---|---|---|---|
| 112 | | | | $4.3^{4}$* | |
| 103 | $2.80^{4}$ | | $1.0^{4} \pm 1.0^{3}$ | | |
| 101 | 3.80 | | $7.5^{3} \pm 8.0^{2}$ | | |
| 99 | 4.80 | | $5.5^{3} \pm 6.0^{2}$ | $1.8^{4}$** | |
| 97 | 6.20 | $4.0^{3} \pm 5.0^{2}$ | $4.0^{3} \pm 5.0^{2}$ | | |
| 95 | 8.00 | $2.5^{3} \pm 5.0^{2}$ | $2.7^{3} \pm 5.0^{2}$ | | |
| 93 | $1.04^{5}$ | $1.8^{3} \pm 4.0^{2}$ | $2.3^{3} \pm 3.0^{2}$ | $1.0^{4} \pm 2.0^{3}$ | |
| 91 | 1.35 | $1.2^{3} \pm 3.0^{2}$ | $1.9^{3} \pm 3.0^{2}$ | $6.0^{3} \pm 1.5^{3}$ | |
| 89 | 1.80 | $7.5^{2} \pm 1.5^{2}$ | $1.4^{3} \pm 2.0^{2}$ | $2.3^{3} \pm 7.0^{2}$ | |
| 87 | 2.45 | $3.5^{2} \pm 1.0^{2}$ | $6.0^{2} \pm 1.0^{2}$ | $1.0^{3} \pm 3.0^{2}$ | $1.9^{3} \pm 5.0^{2}$ |
| 86 | 2.90 | $2.4^{2} \pm 1.0^{2}$ | $2.5^{2} \pm 1.0^{2}$ | $7.0^{2} \pm 1.5^{2}$ | $6.8^{2} \pm 2.0^{2}$ |
| 85 | 3.45 | $1.7^{2} \pm 5.0^{1}$ | $1.5^{2} \pm 1.0^{2}$ | $5.4^{2} \pm 1.0^{2}$ | $3.5^{2} \pm 1.5^{2}$ |
| 84 | 4.10 | $1.4^{2} \pm 5.0^{1}$ | $8.0^{1} \pm 5.0^{1}$ | $2.3^{2} \pm 7.0^{1}$ | $2.4^{2} \pm 1.0^{2}$ |
| 83 | 4.90 | $1.3^{2} \pm 5.0^{1}$ | $5.0^{1} \pm 5.0^{1}$ | $1.5^{2} \pm 5.0^{1}$ | $2.0^{2} \pm 1.0^{2}$ |
| 82 | 5.80 | $1.2^{2} \pm 5.0^{1}$ | $4.0^{1} \pm 5.0^{1}$ | $1.0^{2} \pm 5.0^{1}$ | $1.6^{2} \pm 7.5^{1}$ |
| 80 | 8.10 | $9.0^{1} \pm 5.0^{1}$ | $3.5^{1} \pm 5.0^{1}$ | $9.0^{1} \pm 5.0^{1}$ | $1.2^{2} \pm 7.5^{1}$ |
| 78 | $1.12^{6}$ | | | $8.0^{1} \pm 5.0^{1}$ | $8.5^{1} \pm 5.0^{1}$ |
| 76 | 1.55 | | | $7.0^{1} \pm 5.0^{1}$ | $4.0^{1} \pm 5.0^{1}$ |

*Determined from extinction of 1865 kHz ordinary mode.

**Determined from extinction of 1865 kHz extraordinary mode.

same solar zenith angle. In Tables I and II the uncertainty assigned to an electron density is due primarily to the spread between the results of measurements on the ordinary and extraordinary polarization modes. For small values of electron density somewhat greater weight was given to the results from the extraordinary mode, this mode having the larger amount of absorption.

Some external checks on our 1970 twilight electron density results are given in Table III. Here are compared the computed and measured values of the virtual height of reflection of the ordinary component of a 535 kHz wave. These virtual height measurements (Gnanaligam, 1970, private communication) were made at Colombo, Ceylon (Lat. 6.90°N; Long. 79.87°E) simultaneously with our rocket shots at Thumba (Lat. 8.54°N; Long. 76.86°E). The computed virtual height is defined as $h' = \int_0^h dz/\mu(z)$, where $\mu(z)$ is the refractive index determined from the profiles of Table II and h is the true height of reflection of the 535 kHz wave.

TABLE III

| L.S.T. | $\chi$ (Thumba) | h' (Table II) (km) | h' (Colombo) (km) |
|---|---|---|---|
| 18:12 | 86° | 92.4 | 95 ± 3 |
| 18:36 | 92° | 103.9 | 99 ± 3 |
| 19:00 | 98° | 100.2 | 101 ± 3 |

This comparison is satisfactory, considering the uncertainty on the electron density values in Table II.

An additional check on our 1970 twilight results is provided by the Thumba ionosonde concurrent determination of $f_0E$ (i.e., the maximum electron density of the E-region). In Figure 3 the electron densities of Tables I and II are shown together with the ionosonde determination of the maximum electron density in

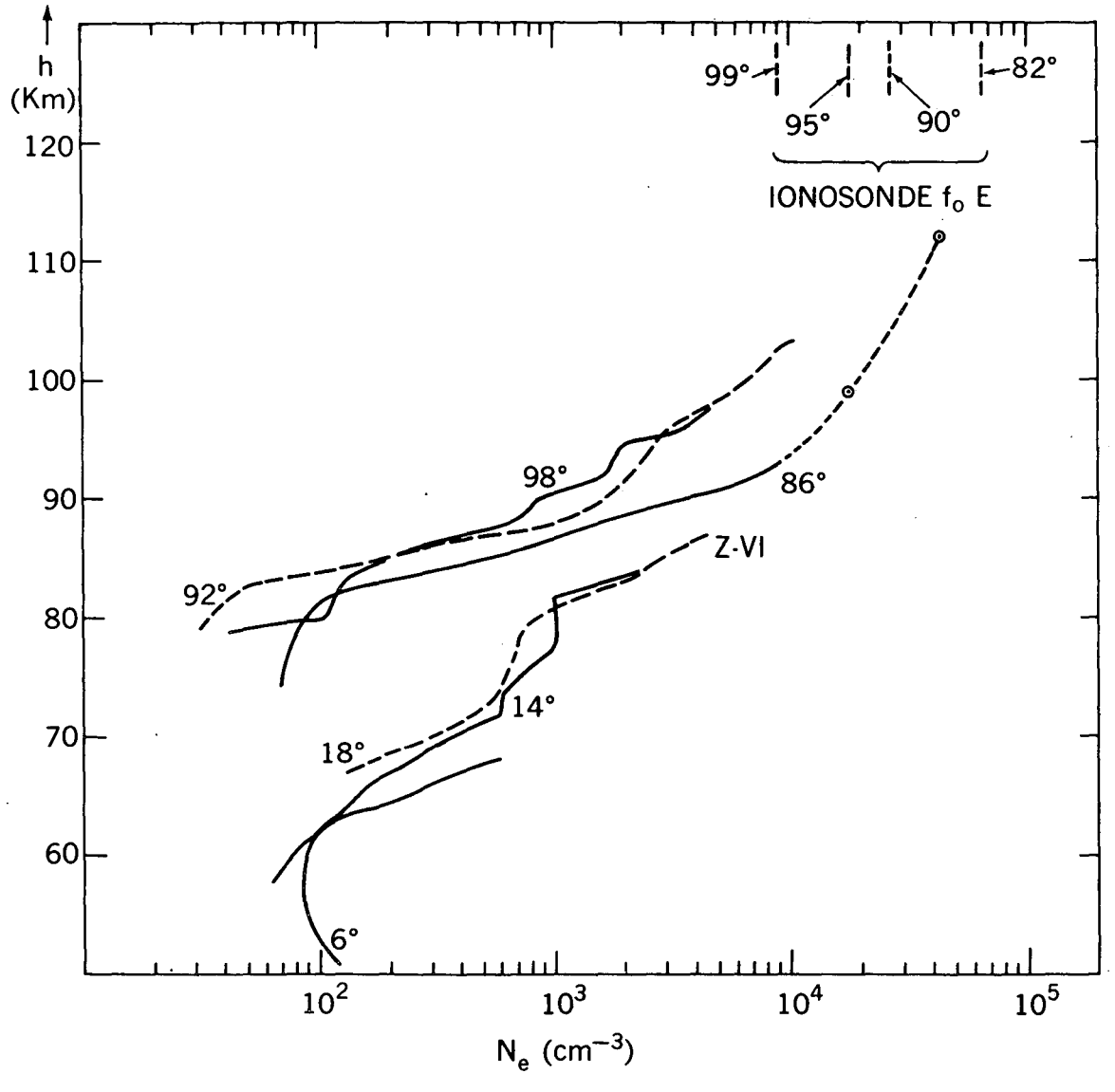


Figure 3. Electron density profiles obtained at Thumba for several solar zenith angles. Profile labeled Z-VI is a mid-latitude result included for comparison. An external check on the twilight profiles is provided by the Thumba ionosonde determination of $F_0$ E, (i.e., the maximum electron density in the E-region).

the E-region during twilight. In Figure 3 it is interesting to note that at 95 km the electron density undergoes a large change between $\chi$ = 86° and 92° but little change between $\chi$ = 92° and 98°. Also in Figure 3, a mid-latitude profile obtained from a Faraday rotation measurement in Greece (Kane, 1969) is shown for comparison purposes. For the two profiles of comparable solar zenith angle but different

latitudes, good agreement is obtained throughout the entire D-region. At small values of solar zenith angle (i.e., when $dN_e/dt \simeq 0$) the buildup of electron density beginning at about 65 km can be directly associated with the corresponding buildup in the profile of the ion production function. Calculated profiles of q, the ion production function, are shown in Figure 4 for the solar zenith angles of interest here. The reason for the above mentioned behavior of the electron density

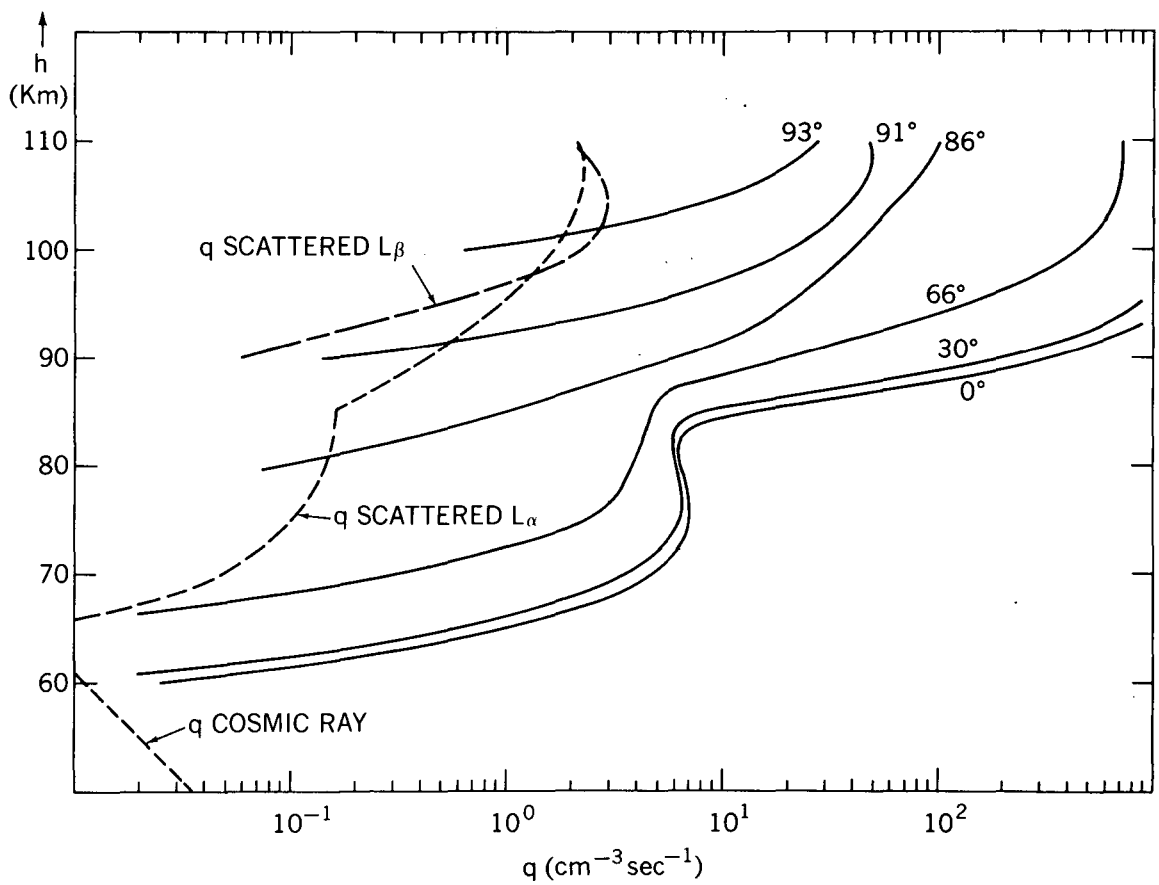


Figure 4. Ion production function q(h) calculated for several solar zenith angles. Calculation includes the following effects: (1) Ionization of nitric oxide (Miera 1970) by Lyman alpha, (2) Lyman beta and soft x-rays in the 31-62 Å wavelength interval (Ohshio et al., 1966; Hinteregger et al., 1965). (3) An integrated energy flux $2 \times 10^{-4}$ ergs $cm^{-2}$ $sec^{-1}$ in the 1-8 Å wavelength interval fitted to an exponential spectral distribution (Elwert, 1961) at a coronal temperature of $T = 2.8 \times 10^6$ deg. The incident scattered Lyman alpha flux is $10^{10}$ photons $cm^{-2}$ $sec^{-1}$ (Mier and Mange, 1970) and the incident scattered Lyman beta flux is $10^7$ photons $cm^{-2}$ $sec^{-1}$ (Ogawa and Tohmatsu, 1966).

at 95 km is now apparent from the behavior of the q function at that altitude. From Figure 4 we also note that below 83 km the ion production function remains constant for solar zenith angle values of $\chi \geq 86$. We shall have occasion to return to this point in the discussion of our positive ion results in section 3.7.

## 3. POSITIVE ION DENSITY MEASUREMENTS

### 3.1 Statement of the Problem

In order to understand the role of negative ions in the D-region electron production and loss processes, quantitative values are necessary. It is therefore highly desirable that electron density measurements be complemented with reasonably accurate measurements of the positive ion density profile. Here by reasonably accurate we mean determining the ion density profile to the order of ±25%. This has proved to be a difficult experimental problem. It is one thing to measure an ion current to a rocket borne probe but quite another to accurately relate that current to the ambient ion density. There are two reasons for this difficulty. At an altitude $h \gtrsim 90$ km the current measured by any plasma probe is strongly dependent on the vehicle potential. In general this quantity is altitude dependent, being a complicated function of electron density and temperature, photoemission current, vehicle velocity, etc. It is therefore not generally valid to infer a positive ion profile by simply normalizing probe data to a known electron density at an altitude where negative ions are negligible. It is of course possible to measure and account for the vehicle potential but only at altitudes above $\simeq$100 km. At these high altitudes however the positive ion density is identical to the electron density and hence of no additional interest. In the low altitude region below $\simeq$ 85 km attention must be given to the effects produced by the formation of shock fronts around the probe. In the sections to follow we describe our efforts and findings thus far concerning these two difficult problems.

3.2 Method of Measurement

For the measurement of the positive ion density a modified Gerdien condenser was used. This device in its idealized form consists of two concentric cylinders between which is maintained a determined flow of ionized air. With the appropriate electric field between the two cylinders the current to either reaches a saturation value $I_s$ which is a simple function of the ion density $N_+$, namely:

$$I_s = N_+ e v A \qquad (3.2:1)$$

where v is the effective velocity of the ion flow across the area A of the Gerdien entrance aperture. We shall consider this velocity term in more detail in section 3.3.

The Gerdien was located axially in the nose of the rocket where it had, after ejection of the clam shell at 60 km, an unobstructed exposure to the air stream during rocket ascent. The geometry of the Gerdien together with its protective clam shell can be seen in Figure 5a. The outer cylinder of the Gerdien (Figure 5b) was electrically connected to the rocket ground while the interior collecting electrode was biased at a negative 25 volts. In laboratory test plasmas this magnitude of bias voltage was sufficient to produce saturation current for gas pressures corresponding to altitudes above 50 km provided the resulting electric field was prevented from fringing to the region outside the Gerdien. It was found that this was accomplished when both the entrance and exit apertures were electrically sealed by means of two grounded grids separated by approximately 3 mm. In the laboratory test plasma we could not simulate the effects of rocket velocity. However a simple calculation shows ion transit time through the Gerdien to be long compared with the maximum time required for the Gerdien electric field to drive to the collector an ion undergoing collisions. Based on this comparison, our

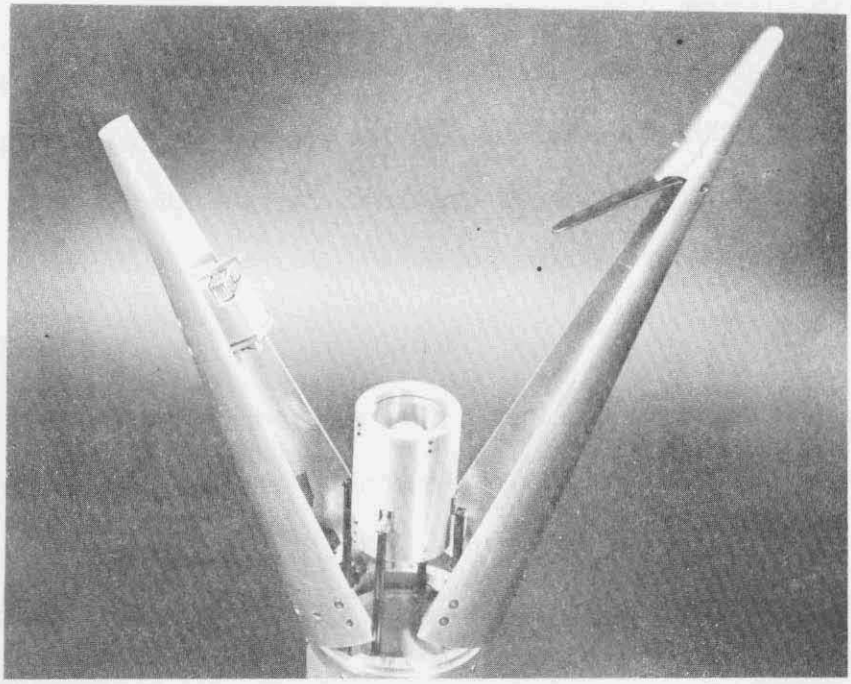

Figure 5a. Geometry of Gerdien probe and protective clam shell.

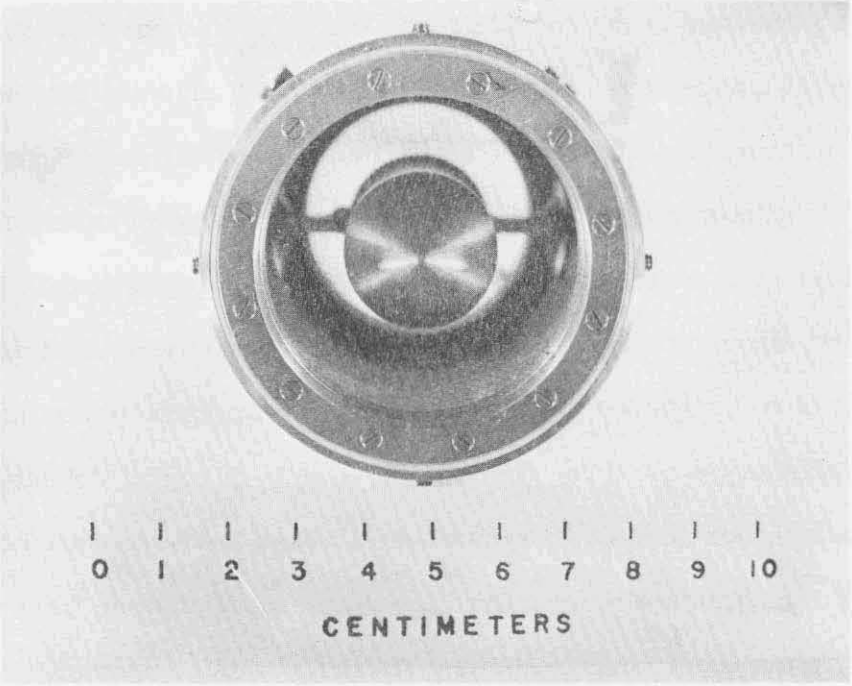


Figure 5b. Interior ion collector electrode is biased 25 volts negative with respect to outer cylinder (i.e. rocket ground).

Gerdien should capture all positive ions of mass $\leq$ 100 AMU at altitudes $\geq$ 50 km for rocket velocity $\leq$ 1 km sec.

3.3 Effective Ion Flow Velocity

We return now to the question of the proper expression for the effective velocity term in equation (3.2:1). In the absence of any electric fields the flow of ions into the Gerdien is the result of the rocket's ramming motion superimposed on an ambient effusive flow process. Consider a unit area that moves with a velocity $v_R$ in a direction which is inclined at an angle $\alpha$ to the area normal. The problem is to calculate the flux of particles crossing this area as it moves through a Maxwellian gas. An elegant treatment of this problem has been given by Tsien (1946). Accordingly, the ion flux into our Gerdien is given by his expression

$$I_s = N_+ e A \frac{v_m}{2\sqrt{\pi}} \left\{ e^{-x^2} + 2\sqrt{\pi}\, x \, \frac{(1 + \text{erf}\,(x))}{2} \right\} \qquad (3.3:1)$$

where $v_m$ is the ion most probable velocity which is given by $Mv^2 = 2\,kT$, with M and T being the ion mass and temperature respectively.

$$x = (v_R \cos\alpha)/v_m \qquad (3.3:2)$$

$$\text{erf}\, x = \frac{2}{\sqrt{\pi}} \int_0^x e^{-y^2}\, dy \qquad (3.3:3)$$

We note that in the limiting cases for $x \to \infty$, and $x \to 0$ we have the familiar expressions:

$$I_s = N_+ e A\, v_R \cos\alpha \qquad v_R \cos\alpha >> v_m \qquad (3.3:4)$$

$$I_s = N_+ e A \frac{v_m}{2\sqrt{\pi}} \equiv N_+ e A \frac{\overline{v}}{4} \qquad v_R \cos\alpha \to 0 \qquad (3.3:5)$$

Equation (3.3:4) is the conventional Gerdien condenser expression for the saturation current associated with a gas flow velocity $v_R$. Equation (3.3:5) will be recognized as the kinetic theory expression for the flux of particles crossing an area A from one side.

3.4 Effect of Shock Front

Equation (3.3:1) is based on the assumption that the Gerdien aperture acts as a sink for any arriving particle, i.e., no particles are reflected at the Gerdien surface. In the realistic situation however, reflected particles are always present. In the free molecular flow regime (i.e., above $\sim$ 85 km) the reflected particles collide so infrequently with the incident particles that no physical effects are produced. However at altitudes where the molecular mean free path is less than the characteristic dimension of the Gerdien probe (i.e., below $\sim$ 85 km) these reflected particles form the well known shock front associated with a supersonic rocket velocity. Figure 6 shows the shock fronts produced by our Gerdien in wind tunnel tests. A calculation given in Appendix A-1 indicates that the effect of the shock front on our measured Gerdien current is not serious, being of the order of 25% or less at altitudes above 70 km. It is planned to test this point further during our next rocket campaign by comparing the results of two identical Gerdiens launched simultaneously, one Gerdien payload being supersonic the other subsonic at the same altitude $\simeq$ 75 km.

3.5 Effect of Vehicle Potential

In Appendix A-1 it is estimated that shock wave effects introduce into our ion measurements errors which are of the order of 25% or less at altitudes above 70 km. At the higher altitudes above 85 km a much larger source of error is the vehicle potential. As shown in Appendix A-2 we can expect a significant error

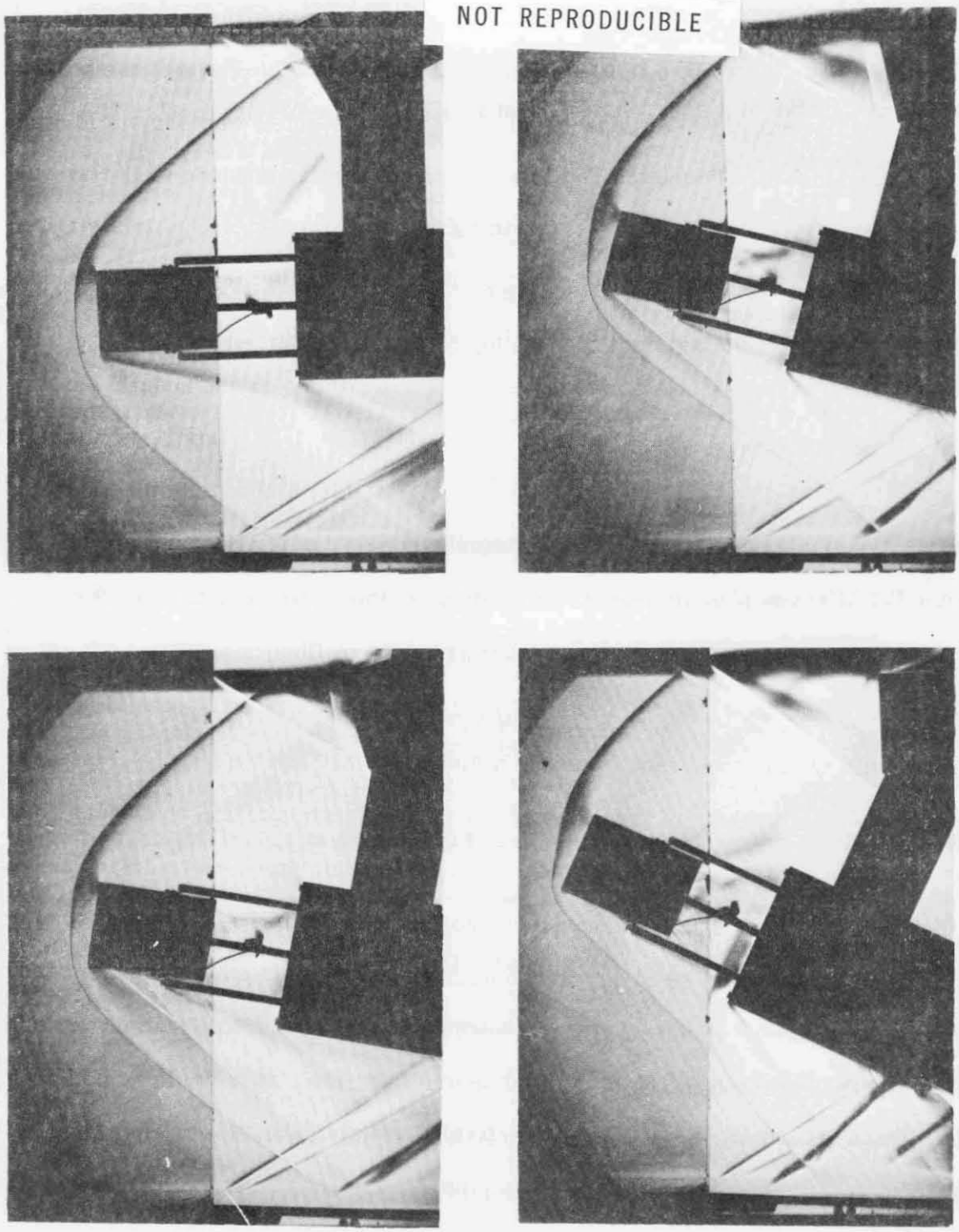

Figure 6. Wind tunnel tests showing shock front formed ahead of Gerdien aperture at several angles of attack, all at Mach 2.

when the vehicle potential is comparable to the relative kinetic energy of an ion approaching the Gerdien.

In the rest frame of a supersonic rocket an ion of mass $M_+$ approaches the rocket with a kinetic energy K.E. given by

$$\text{K.E.} = \frac{1}{2} M_+ v_R^2 \tag{3.5:1}$$

At 70 km our rocket velocity $v_R \simeq 1.0$ km/sec, while at 110 km near peak of the rocket trajectory $v_R \simeq 0.5$ km/sec. For an ion of $M_+ = 30$ AMU we have then

$$\text{K.E.} \simeq 0.16 \text{ eV at } z = 70 \text{ km} \tag{3.5:2}$$

$$\text{K.E.} \simeq 0.04 \text{ eV at } z = 110 \text{ km} \tag{3.5:3}$$

At the higher altitudes where sufficient ambient electron density exists to overcome the effect of photoemission, the vehicle potential can be estimated for the case of a stationary vehicle by using the expression of Chopra (1961)

$$e\phi = kT_e \ln \left( \frac{M_+ T_e}{m_e T_+} \right)^{1/2} \tag{3.5:4}$$

Between 70 and 110 km we can take the ion and electron temperature $T_+ = T_e = 240 \pm 40°K$. This gives then for $M_+ = 30$ AMU

$$e\phi = -0.10 (1 \pm .2) \text{ eV.} \tag{3.5:5}$$

We see immediately that at the higher altitudes the magnitude of the vehicle potential is comparable to or greater than the approaching ion's relative kinetic energy. We can therefore expect this attractive potential of the vehicle to produce a significant enhancement in the ion flux that enters our Gerdien at the higher altitudes.

In the lower altitudes where there are few ambient electrons, photoemission could place the vehicle potential in the range $-0.10 \leq e\phi \leq +2.0$ eV. This estimate of the photoemission effect is made in Appendix A-3. In Appendix A-2 however, it is shown that such a magnitude of vehicle potential would have a negligible effect at the lower altitudes where $\nu >> \nu_0$. Here $\nu_0^2 \equiv e\phi/2m\lambda_0^2$ is a characteristic collision frequency determined by the magnitude of the vehicle potential $e\phi$, the ion mass m, and the characteristic length $\lambda_0 \simeq 5$ cm associated with the dimensions of our Gerdien. In our case (see Appendix II) $\nu_0$ occurs typically at 93 km.

3.6 Mid-Latitude Result

Before presenting the Thumba results obtained at twilight when the photon flux, electron density and vehicle potential are all rapidly changing, let us examine the ion density profile obtained with the same experiment performed at Wallops Island, Virginia, 29 January 1971, 14:48 hr E.S.T., when the solar zenith angle was 66°. This result is presented in Figure 7 together with the simultaneously measured electron density profile. At the lower altitudes the electron density profile was determined by Faraday rotation and absorption measurements on ground-to-rocket radio transmissions at frequencies of 2.3 and 3.0 MHz. These transmissions yielded the electron density up to 88 km plus one point at 103 km where the critical reflection of the 2.3 MHz ordinary component could be identified. Using the $N_+$ profile to interpolate the electron density profile between 88 and 103 km, the Wallops Island ionogram was used to obtain the electron density above 103 km. (To deduce a true height profile from an ionogram it is necessary to know the profile below the height where the lowest frequency ionogram echo appears.) It can be seen in Figure 7 that above 103 km the Gerdien $N_+$ values

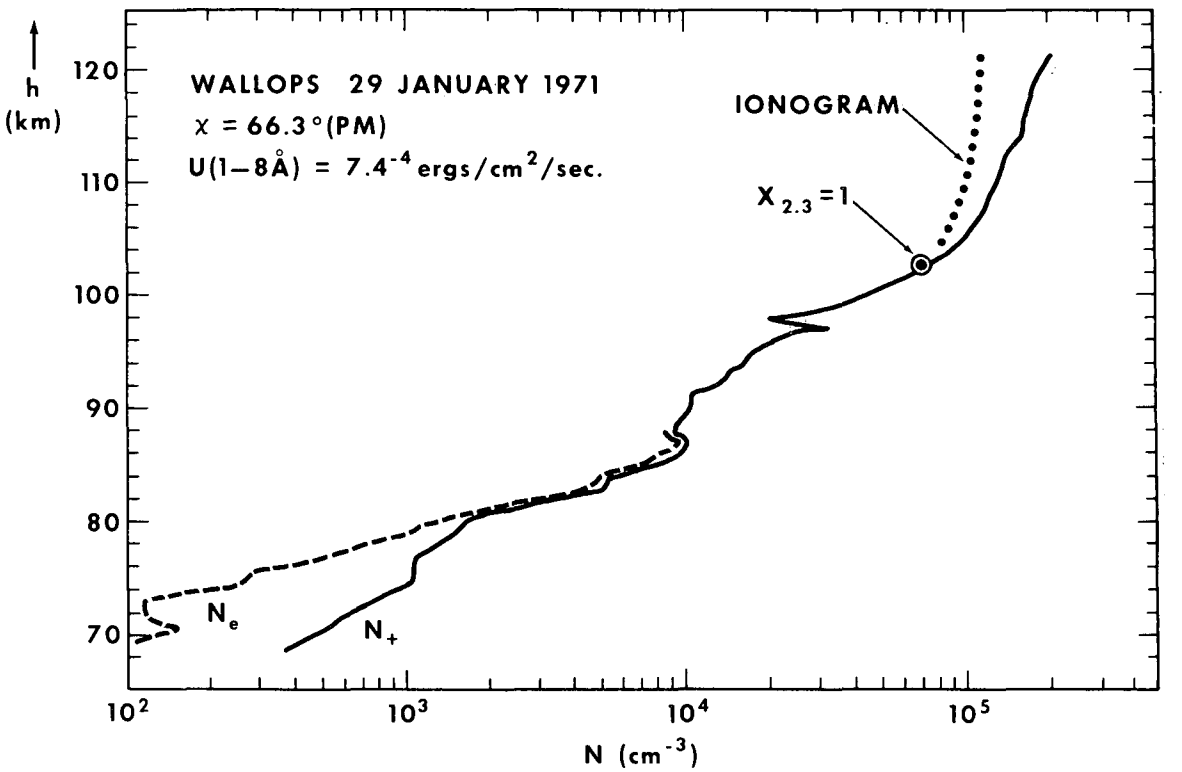


Figure 7. Comparison of Gerdien positive ion profile with simultaneous radio measurement of electron density profile under quasi-equilibrium conditions. This result was obtained at Wallops Island, Virginia, on 29 January 1970, 14:48 hrs E.S.T.

become increasingly greater than $N_e$, approaching a difference of a factor of two at 120 km. This discrepancy cannot be due to an uncertainty in the value of the rocket angle of attack. At apogee, changing the angle of attack in equation (3.3:2) from its value of 80° to 0° produces only a 20% decrease in the deduced value of $N_+$. It is conceivable that the screening of the electric field of the Gerdien collector electrode is not as efficient as our laboratory tests indicated. However as was pointed out in section 3.5 the presence of a negative vehicle potential is a more plausible reason for the high $N_+$ values above 100 km.

Between 70 and 80 km in Figure 7 the difference in the $N_+$ and $N_e$ values can be ascribed to negative ions. This difference represents a lower limit on the

negative ion density since in this altitude region our Gerdien measurement of $N_+$ is a lower limit on the positive ion density. It is of interest at this point to estimate an upper limit to the positive ion density. This can be done from the familiar equation

$$dN_+/dt = q - \alpha_d N_+ N_e - \alpha_i N_+ N_- \qquad (3.6:1)$$

where q is the ion production function and $\alpha_d$, $\alpha_i$ are the coefficients for ion-electron and ion-ion recombination respectively. At $\chi = 66°$ with $dN_+/dt \simeq 0$ (i.e., quasi-equilibrium conditions at 14:48 hrs E.S.T.) we have

$$N_+ = q/\alpha_d N_e \frac{1}{[1 + (\alpha_i/\alpha_d)(N_-/N_e)]} \leq q/\alpha_d N_e \qquad (3.6:2)$$

At 75 km solar Lyman alpha acting on the nitric oxide density (Meira, 1970) yields at $\chi = 66°$ the value $q = 2.4$. Under these quasi-equilibrium conditions the dominant positive ion is $37^+$ (Narcisi, 1967; Goldberg, 1971) for which $\alpha_d = 5 \times 10^{-6}$ (Aikin et al, 1971). These values of q and $\alpha_d$ together with the value $N_e = 3 \times 10^2$ (Figure 7) inserted into equation (3.6:2) yield the upper limit on the positive ion density at 75 km

$$N_+ \leq 2 \times 10^3 \qquad (3.6:3)$$

Comparing this with our measured lower limit

$$N_+ \geq 1 \times 10^3 \qquad \text{(measured)} \qquad (3.6:4)$$

we see that our Gerdien measurement of positive ion density are consistent with the independent D-region measurements of ion mass spectroscopy and nitric oxide density, together with the laboratory value of the ion recombination coefficient.

Having shown how our Gerdien performs under stable ionospheric conditions (i.e., when $dN_e/dt \simeq 0$), we can now consider the results of our twilight measurements at Thumba.

3.7 Thumba Results

In Figure 8 for each of the three solar zenith angles 98°, 92° and 86°, the Gerdien $N_+$ profile is compared with the corresponding electron density profile. At $\chi = 98°$ the values of $N_+$ above 100 km are in very good agreement with the ionogram determination of $f_0E$, the maximum electron density of the E region. This agreement indicates that at this zenith angle a negligible vehicle potential is present in this high altitude region and presumably at the lower altitudes as well, since no photoelectric effect would be expected at this solar zenith angle. The observed difference between the $N_+$ and the $N_e$ profiles for this zenith angle can then be attributed to the presence of negative ions. At the sunset value of $\chi = 98°$ a significant number of negative ions are seen to exist at least as high as 95 km. Similar evidence for the presence of negative ions at these fairly high altitudes during sunrise has been reported by Pedersen and Kane (1971).

At $\chi = 92°$ negative ions are apparently present in significant numbers below 88 km while above that altitude a negative vehicle potential is invoked to explain the discrepancy between the $N_+$ and $N_e$ determinations. The question immediately arises as to why at the high altitudes there should exist a large difference between the $N_+$ and $N_e$ measurements at $\chi = 92°$ but not at $\chi = 98°$. The reason is that at these high altitudes where the time constant for the electrons to thermalize is of the order of some tenths of a second, the vehicle potential is controlled not so much by the thermal electron population as it is by the high energy bump (H.E.B.) that occurs in the distribution function at the energy.

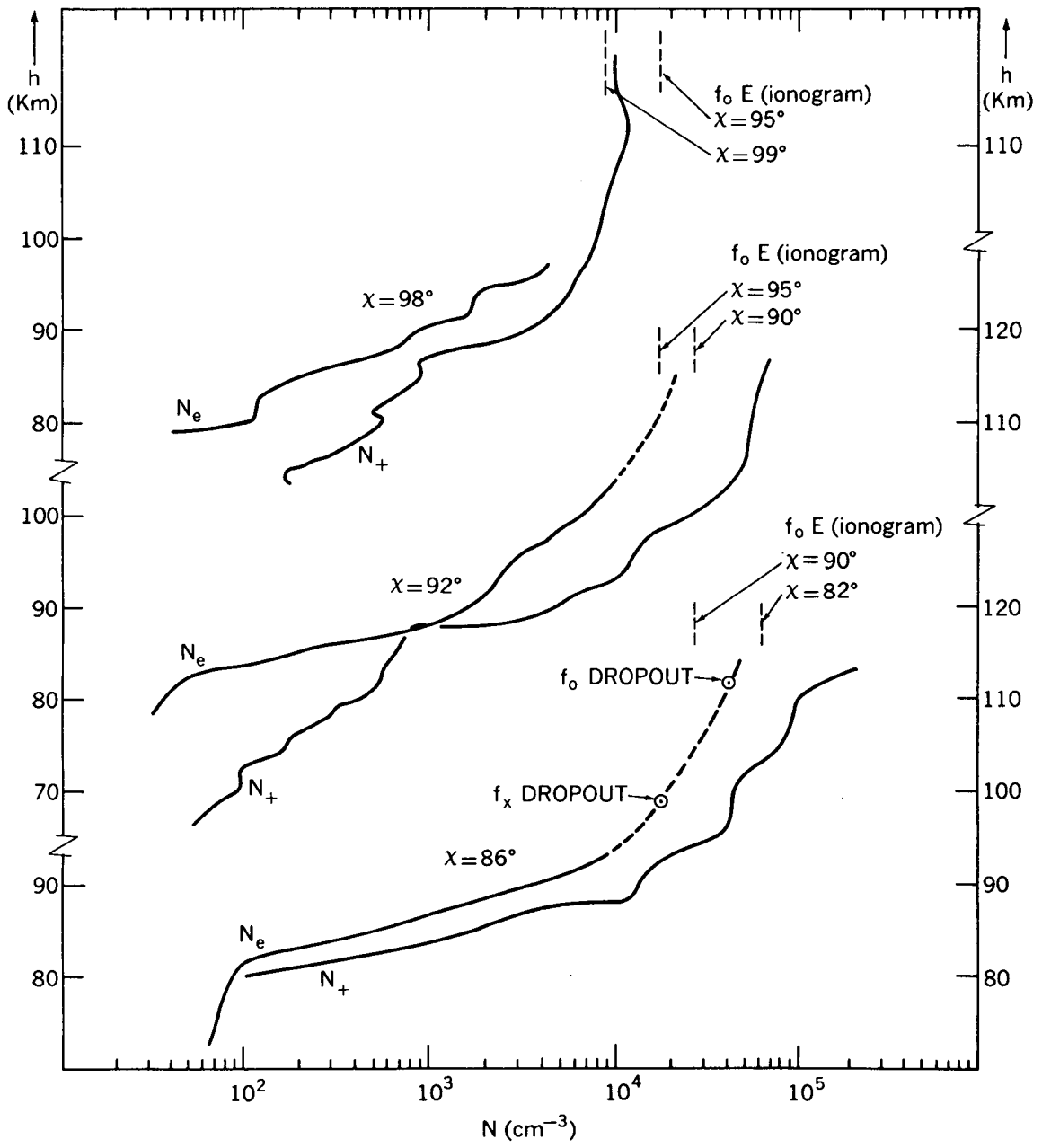


Figure 8. Comparison of Gerdien positive ion results with simultaneous radio measurements of electron density profiles at sunset. .

$$H.E.B. = h\nu - I_p \qquad (3.7:1)$$

Here $h\nu$ is the energy of the incident photon and $I_p$ is the ionization potential of the ionizable constituent. At the solar zenith angles in our case, we are concerned only with the Lyman alpha-nitric oxide process for which H.E.B. = 0.95 eV. The number of H.E.B. electrons will be proportional to the ion production function q. Hence at 110 km where we have (see Figure 4) $q = 40$ at $\chi = 92°$, and $q = 2.5$ at $\chi = 98°$, we would expect a significant reduction in vehicle potential as twilight proceeds through these two values of solar zenith angle.

At $\chi = 86°$ the similarity in the general shape of the $N_+$ and $N_e$ profiles suggests that at this zenith angle negative ions are not present in any significant numbers above 81 km. However the data here is not conclusive on this point since a fortuitous altitude dependent vehicle potential could also explain the observed similarity of the two profiles.

Finally Figure 9 shows the comparison of Gerdien $N_+$ profiles for the three solar zenith angles. The surprising feature seen here is that below 83 km the positive ion density appears to increase with increasing solar zenith angle. Such behavior is not as strange as it might appear to be at first glance. The positive ion density at a given altitude is governed by the familiar equation relating the ion production and loss processes:

$$dN_+/dt = q(t) - \alpha_d N_+ N_e - \alpha_i N_+ N_- \qquad (3.7:2)$$

where $\alpha_d$ & $\alpha_i$ are the respective rate coefficients for the dissociative and ion-ion recombination processes. It is generally believed that $\alpha_d > \alpha_i$. It will be noted in Figure 4 that below $\sim$ 83 km the q function remains constant for $\chi \geq 86°$. In this altitude range during twilight, electrons are lost by forming negative ions

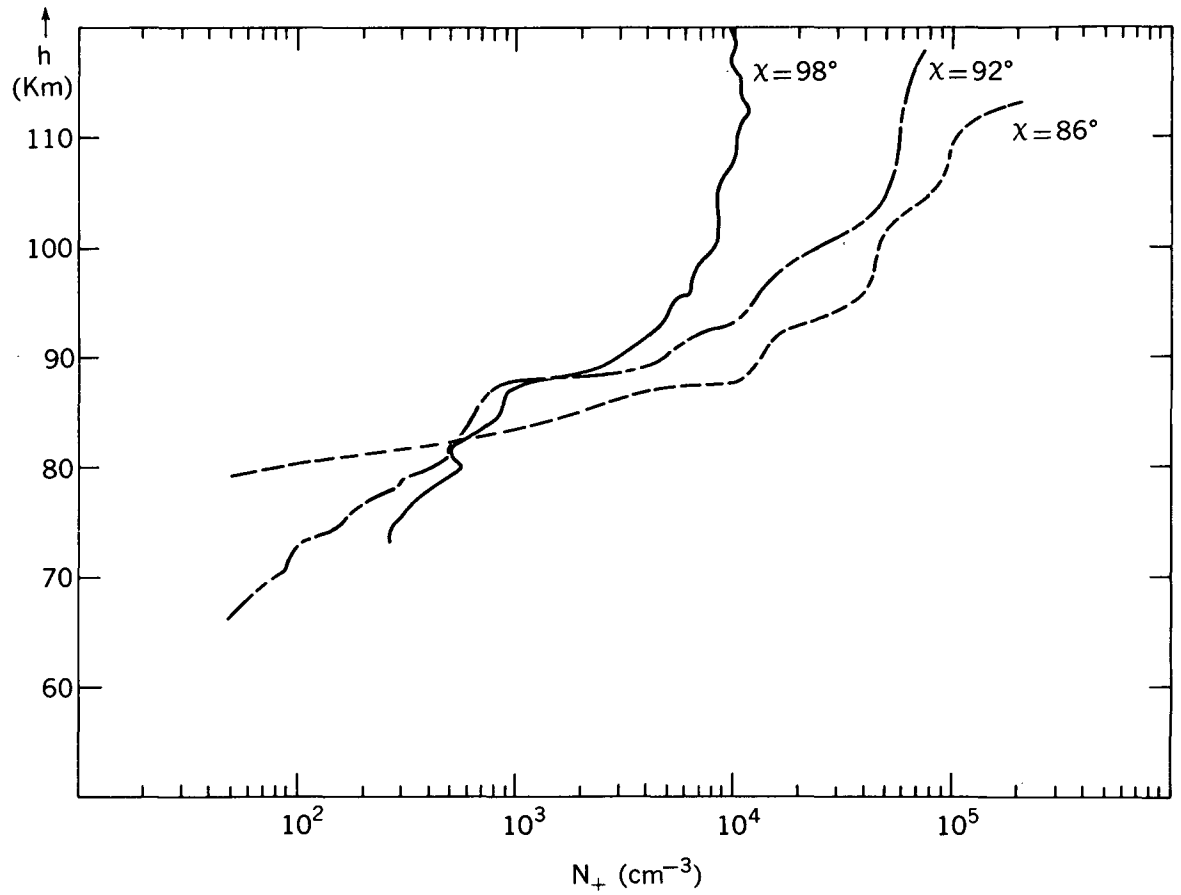


Figure 9. Comparison of Gerdien results at twilight showing a build-up of positive ion density below 83 km as sun goes down.

and are no longer available to dissociatively destroy positive ions. The latter are now lost by the slower ion-ion recombination process. This slow-down of the loss rate in the presence of a constant q function results in a build-up of positive ion density. For a detailed chemistry model of such a process the reader is referred to Turco and Sechrist (1970).

## 4. CONCLUSIONS

### 4.1 Electron Density Measurements

The measurement of cw absorption on frequencies around 2 MHz is a practical method for the determination of electron densities which are greater than

$10^2$ $cm^{-3}$. With this method the altitude to which an electron density profile can be determined is limited by our knowledge of the collision frequency profile. At the present time this means an altitude limit of about 100 km. The method is particularly well suited to the magnetic equator where the characteristic polarization modes can be radiated from simple dipole antennas. However when the electron densities are less than $10^2$ $cm^{-3}$ this method is inadequate. Consequently for problems such as the D-region at nighttime or during a solar eclipse, further studies of the electron production and loss process will require a more sensitive radio technique to supplement and evaluate probe measurements of positive ion density.

4.2 Positive Ion Density Measurements

Accurate measurements of positive ion densities are difficult. Special care must be taken in evaluating vehicle potential effects, especially during non-equilibrium conditions. Above 90 km, depending on the magnitude of the vehicle potential, Gerdien probe measurements of positive ion densities could be in error by as much as a factor of two. Hence to normalize ion probe data to a high altitude electron value is not a valid procedure. Below 85 km vehicle potential effects are not important on a supersonic rocket. In this lower altitude region shock wave effects introduce errors of the order of 25% into our Gerdien probe measurements of positive ion density. Probes of a different geometry however would of course require individual evaluation. With the stated accuracy of 25% in the absence of a significant vehicle potential, the present Gerdien ion trap should be quite adequate for a study of the nighttime lower ionosphere.

4.3 Negative Ions

In the D- and lower E-region direct measurement of $N_-$, the negative ion density, is not practical at the present time. However below the altitude where the vehicle potential begins to affect the Gerdien ion current, the $N_-$ profile can be inferred from the difference in the $N_+$ and $N_e$ measurements. This cut-off altitude will vary with ionospheric conditions but typically it will be above 85 km.

From the electron and positive ion results shown in Figure 8 we have the following qualitative description of the negative ion situation at twilight. At $\chi$ = 86° some negative ions, of the order of 500 $cm^{-3}$, might be present between 80 and ~ 85 km. Unfortunately our data in this instance does not allow an unambiguous assessment of the vehicle potential effect. At $\chi$ = 92° however, negative ions are clearly present in significant numbers below 88 km, while at $\chi$ = 98° significant numbers of negative ions extend to at least 95 km.

Now that the feasibility of such negative ion density measurements has been demonstrated, further effort must concentrate on making both electron and positive ion density measurements as accurately as possible. Until this is done only limited progress in understanding the negative ion chemistry of the ionosphere can be expected.

ACKNOWLEDGEMENTS

This work was made possible through an international cooperative program between NASA and ISRO. We are especially grateful to H. G. S. Murthy, Thumba range director, for valuable assistance with the field operations. W. L. Haynes (GSFC) was responsible for both the rocket borne and ground based scientific instrumentation. Payload fabrication and integration was under the direction of J. C. Modlin (GSFC). The very helpful wind tunnel tests were conducted by R. A. Goldberg (GSFC). The analysis of ionogram records was by J. E. Jackson, (GSFC).

## REFERENCES


Aiken, A. C., R. A. Goldberg and Y. V. Somayajulu, "Electron and Positive Ion Density Altitude Distributions in the Equatorial D-Region", Goddard Document X-625-71-308, August 1971.

Arnold, F., J. Kissel, D. Krankowski, H. Wieder, and J. Zahringer, "Negative Ions in the Lower Ionosphere: A Mass Spectrometric Measurement", J. Atmos. Terr. Phys. 33, 1169-1175, August 1971.

Chopra, K. P., "Interactions of Rapidly Moving Bodies in Terrestrial Atmosphere", Rev. Mod. Phys. 33, 2, 153-189, April 1961.

Elwert, G., "Theory of X-Ray Emission of the Sun", J. Geophys. Res., 66, 2, 391-401, February 1961.

Feuerbacher, B. and B. Fitton, "Experimental Investigations of Photoemission From Satellite Surface Materials", ESRO Surface Physic Division, unpublished report, 1971.

Gnanalingam, S., "Ionospheric Absorption at Low Latitudes", Proceedings of the Third International Symposium on Equatorial Aeronomy, Ahmedabad, India, Vol. I, pp. 47-69, February 1969.

Goldberg, R. A., "Positive Ion Composition Measurements in the D- and E-Regions of the Equatorial Ionosphere", Goddard Document X-625-71-258, July 1971.

Grard, R. J. L., and J. K. E. Tunaley, "Photoelectron Sheath Near a Planar Probe in Interplanetary Space", J. Geophys. Res., 76, 10, 2498-2505, April 1971.

Hale, L. C., D. P. Hoult and D. C. Baker, "A Summary of Blunt Probe Theory and Experimental Results", Space Res. VIII, North Holland Publishing Co., Amsterdam, 1968.

Hinteregger, H. E., L. A. Hall and G. Schmidtke, "Solar XUV Radiation and Neutral Particle Distribution in July 1963 Thermosphere", Space Res. V, 1175-1190, North-Holland Publishing Co., Amsterdam, 1965.

Hudgins, J. I. and J. R. Lease, "Tone Range-Telemetry Tracking System for Support of Sounding Rocket Payload", NASA SP-219, pp 187-226, 1969.

Kane, J. A., "D-Region Electron Density Measurements During the Solar Eclipse of May 20, 1966", Planet. Space Sci., 17, 609-616, 1969.

Kane, J. A., "D Region Radio Measurements at the Magnetic Equator", Goddard Document X-615-69-499, November 1969.

Meier, R. R. and P. Mange, "Geocoronal Hydrogen: An Analysis of the Lyman Alpha Airglow Observed from OGO-4", Planet. Space Sci., 18, 6, 803-821, June 1970.

Meira, L. G., "Rocket Measurements of Upper Atmospheric Nitric Oxide and Their Consequences to the Lower Ionosphere", J. Geophys. Res., 76, 202-212, 1971.

Narcisi, R. S., "Ion Composition of the Mesosphere", Space Res. VII, 186-195, North-Holland Publishing Co., Amsterdam 1967.

Narcisi, R. S., A. D. Bailey, L. Della Luca, C. Sherman and D. M. Thomas, "Mass Spectrometric Measurements of Negative Ions in the D- and Lower E-Region". J. Atmos. Terr. Phys. 33, 1147-1159, August 1971.

Ogawa, T. and T. Tohmatsu, "Photoelectric Process in the Upper Atmosphere, 2, The Hydrogen and Helium Ultraviolet Glow as an Origin of the Nighttime Ionosphere", Rept. Ionosphere Space Res., Japan, 20, 395-417, 1966.

Ohshio, M., R. Maeda and H. Sakagami, "Height Distribution of Local Photo-ionization Efficiency", Journal of the Radio Research Laboratories (Japan) Vol. 13, 70, November 1966.

Pai, S. I., "Introduction to the Theory of Compressible Flow", D. Van Nostrand Co., Inc., Princeton, N.J., 1959.

Pedersen, A., and J. A. Kane, "Rocket Measurements of Ion and Electron Densities in the D- and Lower E-Regions Near Sunrise". ESRO Scientific Note SN-116, March 1971.

Phelps, A. V., "Propagation Constants for Electromagnetic Waves In Weakly Ionized Air", J. Appl. Phys., 31, 1723-1729, 1960.

Sen, H. K. and A. A. Wyller, "On the Generalization of the Appleton-Hartree Magnetoionic Formulas", J. Geophys. Res., 65, 3931-3950, 1960.

Smith, W. S., J. S. Theon, P. C. Swartz, L. G. Katchen, and J. J. Horvath, "Temperature, Pressure, Density and Wind Measurements in the Upper Stratosphere and Mesosphere, 1965". NASA Technical Report TR R-263, 1967.

Tsien, H. S., "Superaerodynamics, Mechanics of Rarified Gases", J. Aeronautical Sci., 13, 12, 653-664, December 1946.

Turco, R. P. and C. F. Sechrist, "An Investigation of the Ionospheric D Region at Sunrise", University of Illinois Aeronomy Rept. No. 41, December 1970.

Whipple, E. C., "The Equilibrium Electric Potential of a Body in the Upper Atmosphere and in Interplanetary Space", NASA-Goddard Report X-615-65-296, June 1965.

## APPENDIX A-1

## EFFECT OF SHOCK FRONT ON GERDIEN CURRENT

Wind tunnel tests of our Gerdien at Mach 2 and several angles of attack (Figure 6) show the shock front to be approximately planar immediately ahead of the Gerdien aperture. To estimate the effect of such a shock on the measured Gerdien current we shall assume that the shock front can be adequately described by a plane which makes an angle $\delta$ with respect to the plane of the Gerdien aperture. Let the undisturbed flow ahead of the shock be described by the gas density $\rho_1$ and the stream velocity $u_1$. $\alpha$ is the angle of attack and $\delta$ lies in the range $0 \leq \delta \leq \alpha$. The velocity vector $\bar{u}_1$ makes the angle $\theta_1$ with respect to the shock front normal, while behind the shock we have the same parameters given by $\rho_2$, $u_2$ and $\theta_2$ (see Figure 1-A-1).

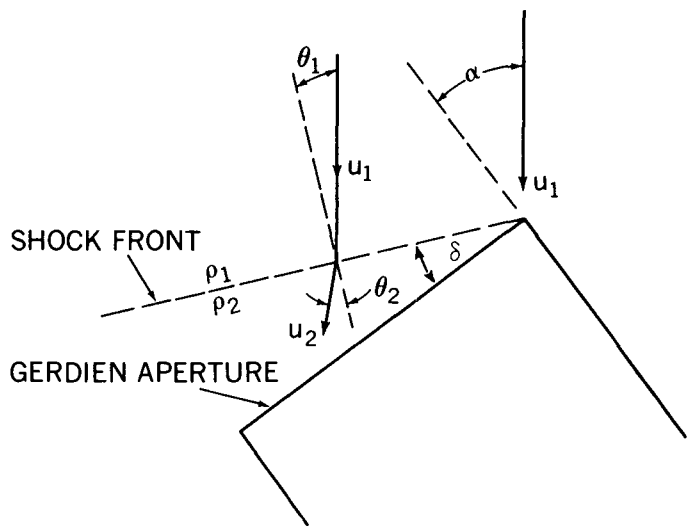


Figure 1-A-1

The continuity equation for mass flow requires that the normal components of $\rho u$ and the tangential components of u be continuous across the shock front.

$$\rho_1 u_1 \cos\theta_1 = \rho_2 u_2 \cos\theta_2 \qquad (1, A\text{-}1)$$

$$u_1 \sin\theta_1 = u_2 \sin\theta_2 \qquad (2, A\text{-}1)$$

A third relationship we shall need is the ratio of gas densities across the shock front. This is given by

$$\rho_1/\rho_2 = \frac{\gamma - 1}{\gamma + 1} + \frac{2}{\gamma + 1}\left(\frac{1}{M_1^2 \cos^2\theta_1}\right) \qquad (3, A\text{-}1)$$

where $M_1$ is the free stream Mach number, and $\gamma$ is the ratio of specific heats. Equation (3) can be derived from a consideration of the energy and momentum relationships in an adiabatic process (see for example Pai, S. I., 1958, pp. 44f).

From Figure 1-A-1 it can be seen that the mass flow $F_G$ into the Gerdien is given by

$$F_G = \rho_2 u_2 \cos(\theta_2 + \delta) \qquad (4, A\text{-}1)$$

$$= \rho_2 u_2 (\cos\theta_2 \cos\delta - \sin\theta_2 \sin\delta) \qquad (5, A\text{-}1)$$

By substitution from equations (1) and (2) together with the geometrical relationship

$$\alpha = \theta_1 + \delta \qquad (6, A\text{-}1)$$

equation (5) becomes

$$F_G = \rho_1 u_1 \cos\alpha \left(1 + \frac{\sin\theta_1 \sin\delta}{\cos\alpha}\left(1 - \frac{\rho_2}{\rho_1}\right)\right) \qquad (7, A\text{-}1)$$

$$F_G = F_G'(1 - \epsilon) \qquad (8, A\text{-}1)$$

where $F_G'$ is mass flow into the Gerdien in the absence of any shock front, and $\epsilon$ is a correction term given by

$$\epsilon = \frac{\sin\theta_1 \sin\delta}{\cos\alpha} (\rho_2/\rho_1 - 1) \qquad (9, A\text{-}1)$$

Finally from (3), taking $\gamma = 1.4$ for diatomic molecules, we have

$$(\rho_2/\rho_1 - 1) = \frac{5M_1^2 \cos^2\theta_1 - 5}{M_1^2 \cos^2\theta_1 + 5} \qquad (10, A\text{-}1)$$

From equations (6), (9) and (10) the correction term $\epsilon$ can be calculated for a range of values of $\delta$ where $0 \leq \delta \leq \alpha$. In this way a maximum value of $\epsilon$ is obtained for a given value of M and $\alpha$. ($\epsilon_{max}$ occurs at a value of $\delta \simeq \alpha/2$.) Figure 2-A-1 shows a family of $\epsilon_{max}$ vs angle of attack for several values of Mach number. From Figure 2-A-1 we conclude that for the normal flight

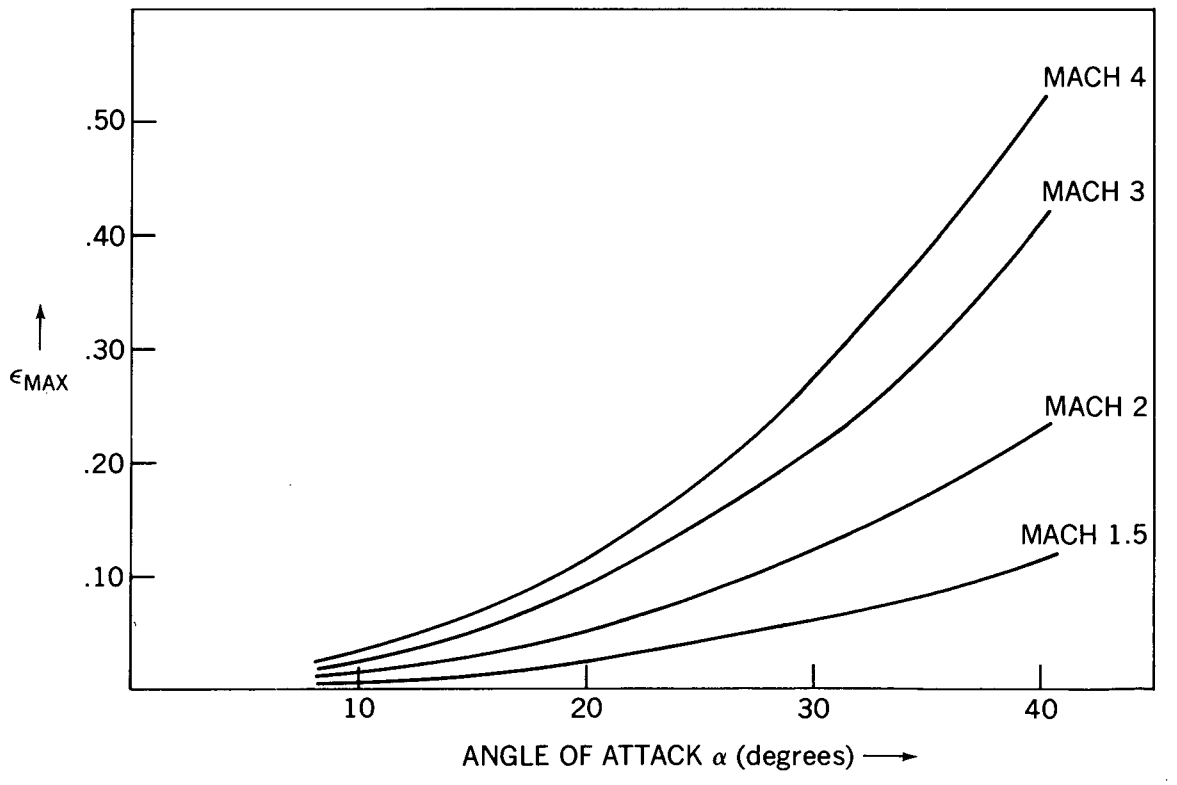


Figure 2-A-1

conditions of our rocket (i.e., $M \leq 3$ and $\alpha \leq 30°$), shock fronts introduce errors of the order of 25% or less into our determination of positive ion density.

## APPENDIX A-2

## EFFECT OF VEHICLE POTENTIAL ON GERDIEN CURRENT

To estimate the effect of the vehicle potential on the measured Gerdien ion current we proceed as follows. In the rest frame of the rocket the approaching ion has an initial velocity $v_0$. The Gerdien cylinder, radius a, being electrically at rocket ground, presents an attractive potential $-e\phi$ to the approaching ion. Due to this negative potential the effective area A′ for ion collection (Figure 1-A-2)

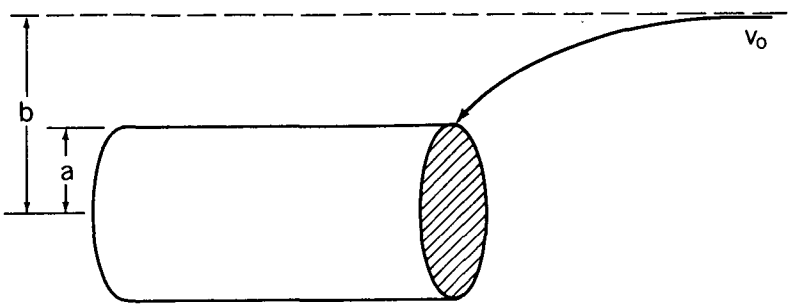


Figure 1-A-2

is given by

$$A' = \pi b^2 = (b/a)^2 A_0 . \qquad (1, A\text{-}2)$$

For simplicity we replace the disk shaped Gerdien entrance aperature (the hatched area in Figure 1-A-2) by a sphere of radius a which is at a potential - $e\phi$. We now have an elementary problem in classical mechanics (Figure 2-A-2). The conservation of angular momentum about the origin of the sphere yields the relation

$$mva = mv_0 b \qquad (2, A\text{-}2)$$

while the conservation of energy gives the relation

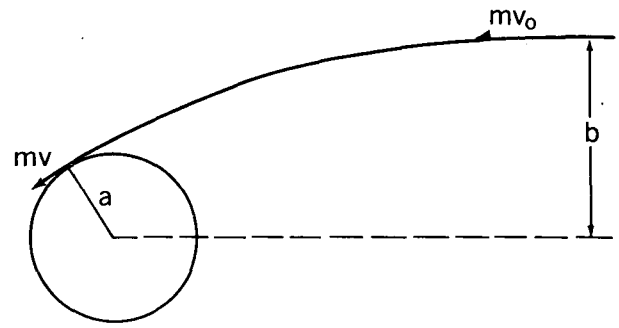


Figure 2-A-2

$$\frac{mv^2}{2} = \frac{mv_0^2}{2} + e\phi \qquad (3, A\text{-}2)$$

or

$$(v/v_0)^2 = 1 + e\phi/\text{K.E.} \qquad (4, A\text{-}2)$$

From equations (4) and (2), the effective Gerdien area for ion collection, equation (1), becomes

$$A' = A_0 [1 + e\phi/\text{K.E.}] \qquad (5, A\text{-}2)$$

where K.E. = 1/2 $mv_0^2$ is the initial kinetic energy of the approaching ion and $A_0$ is the geometrical area $\pi a^2$.

Equation (5) was derived for the case where the ion-neutral collision frequency $\nu = 0$. The effect of a non zero ion collision frequency will be to reduce the Gerdien's dependence on vehicle potential. We can make a rough estimate of this reduction in the effect of the vehicle potential as follows. When $\nu \neq 0$ the ion motion in the attractive potential of the rocket is governed by the equation

$$\dot{v} + \nu v = e/m\, E(r) \qquad (6, A\text{-}2)$$

where E (r) is the electric field associated with the vehicle potential $e\phi$. For our purpose we take a model electric field such that

$$eE = e\phi/\lambda_0 \qquad \text{for } r < \lambda_0 < \lambda_d \qquad (7, A\text{-}2)$$

$$= 0 \qquad \text{for } r > \lambda_0$$

where $\lambda_0 \simeq 5$ cm is a characteristic length associated with the dimensions of our Gerdien, and $\lambda_d$ is the plasma Debye length given by $\lambda_d = 6.9\sqrt{T/N_e}$ (CGS units). For the Thumba twilight conditions below $\simeq$ 90 km $\lambda_d > \lambda_0$. For this reason our model electric field in equation (7) is determined by $\lambda_0$ rather than $\lambda_d$.

If $\tau$ is the transit time for the ion to move through the distance $\lambda_0$, the solution of equation (6, A-2) gives

$$v(\tau) = \frac{e\phi}{m\lambda_0\nu}\left[1 - e^{-\nu\tau}\right] \qquad (8, A\text{-}2)$$

$$= \frac{e\phi}{m\lambda_0\nu} \qquad \nu\tau >> 1 \qquad (9, A\text{-}2)$$

At the end of the time interval $\tau$, the ion arrives at the Gerdien aperture with a kinetic energy $\frac{mv^2(\tau)}{2}$. By means of this kinetic energy we define an equivalent or effective vehicle potential $e\phi'$ to be used when the ion-neutral collision frequency can not be neglected.

$$\frac{m\,v^2(\tau)}{2} = e\phi' = e\phi\,\frac{e\phi}{2\,m\lambda_0^2\nu^2} \qquad (10, A\text{-}2)$$

$$e\phi' = e\phi\,(\nu_0/\nu)^2 \qquad (11, A\text{-}2)$$

Taking $e\phi = 0.10$ eV, $\lambda_0 = 5$ cm and m = 30 AMU, we have $\nu_0 = 7.8 \times 10^3$. This value of $\nu_0$ defines an altitude $\simeq$ 93 km, below which we should replace the $e\phi$ term in equation (5, A-2) by the term $e\phi'$ of equation (11, A-2).

## APPENDIX A-3

## EFFECT OF PHOTOEMISSION ON VEHICLE POTENTIAL

In the absence of an ambient plasma, illumination of the rocket by monochromatic radiation of energy $h\nu$ would charge the rocket to a positive potential

$$e\phi = h\nu - W \qquad (1, A\text{-}3)$$

where W is the work function of the rocket surface material. Since the solar ultraviolet spectrum extends to an arbitrarily high energy, so also would the vehicle potential were it not for the presence of an ambient plasma. If the density of the ambient plasma is not too large, a positive value of equilibrium potential $e\phi$ is established such that the resulting current $i_{am}$ of ambient plasma electrons is equal to the photo current $i_{pho}$ of electrons emitted with energies sufficient to escape the attraction of the vehicle potential, i.e.

$$i_{am} = i_{pho} \equiv \int_{e\phi}^{\infty} j(E)\, dE \qquad (2, A\text{-}3)$$

In equation (2, A-3) the critical parameter in the calculation of $e\phi$ is $j(E)$, the energy distribution function of the photoemitted electrons. Most of the available photoemission data has been obtained from solid state studies where measurements are made on clean samples under ultra-high vacuum conditions. Such clean sample data however is not applicable to the present problem since photoemission properties are so drastically affected by surface contamination from absorbed gases (Grard and Tunaley, 1971; Whipple, 1965).

Recently, for several wavelengths in the 4 to 23 eV range, Feuerbacher and Fitton (1971) have measured the energy distribution functions of photoelectrons emitted from untreated aluminum. Using their laboratory results for untreated

aluminum it is possible to calculate $i_{pho}$ versus $e\phi$ for the case of incident solar radiation. Fortunately for the case of the D-region, due to factors such as the shape of the solar spectrum, atmospheric attenuation, and decreased photo yield at high energy, it is necessary to consider only incident radiation of energy equal to and less than Lyman alpha in the calculation of $i_{pho}$. The result of such a calculation is shown in Figure 1-A-3.

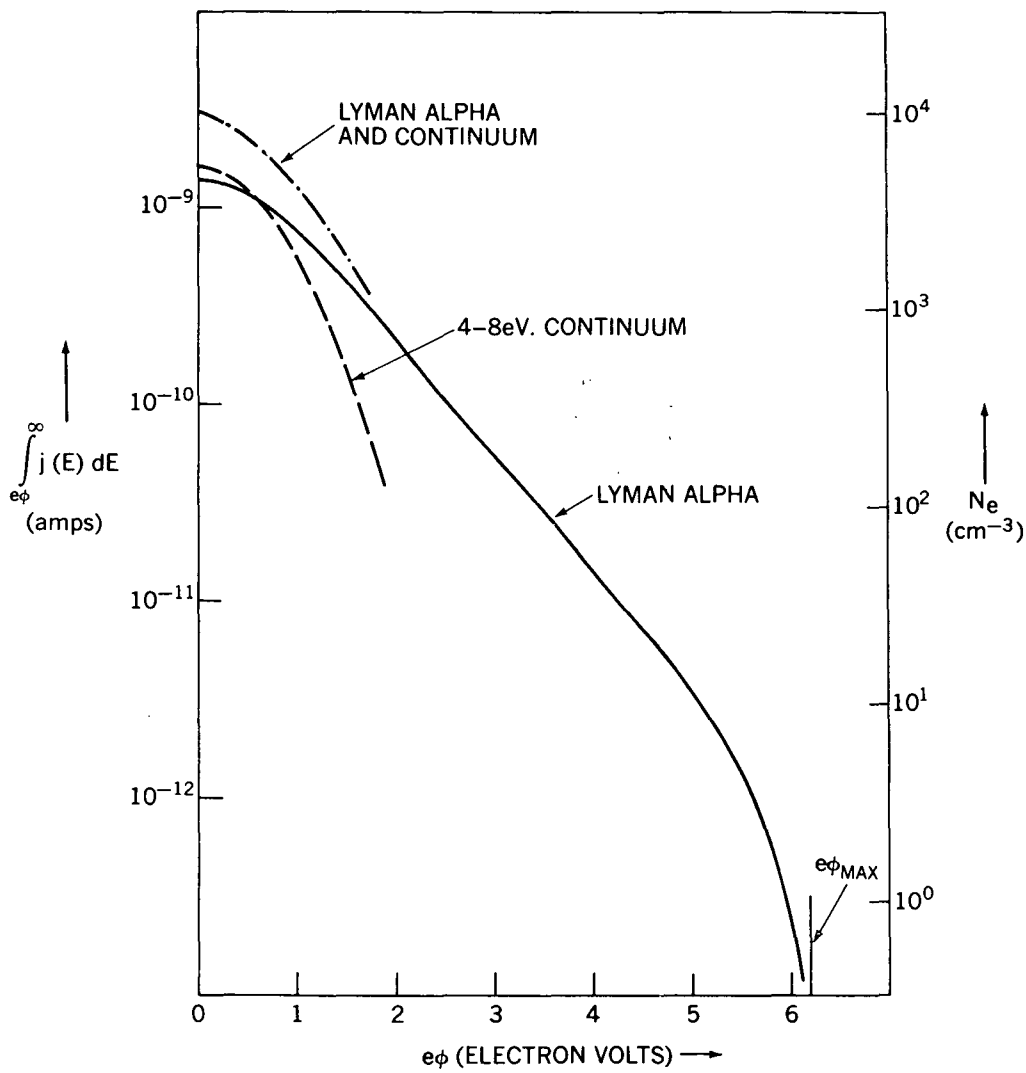


Figure 1-A-3

To interpret this figure it is necessary to note from the work of Feuerbacher and Fitton (loc. cit.) that $i_{pho}$ has effectively two components, each of approximately equal photo yield. These are (1) photoelectrons due to incident Lyman alpha shown in Figure 1-A-3 as the solid curve, and (2) photoelectrons due to the continuum spectra of incident solar photons with energies between 4 and $\simeq 8$ eV. shown as the dashed curve. The lower limit of this continuum at 4 eV. represents the work function of untreated aluminum while the upper limit is due to the rapid fall-off in the solar flux for photon energies greater than $\simeq 8$ eV. From the sum of the two components of $i_{pho}$ at $\phi = 0$ we see that in the D-region the total photoelectric current yield from untreated aluminum is $3 \times 10^{-9}$ amps/cm$^2$. The estimated accuracy on this calculation is of the order of ±50%. This places the calculated value in good agreement with the rocket measurement by Whipple (loc. cit.) who reported $i_{pho}(\phi = 0) = 2.6 \times 10^{-9}$ amps/cm$^2$ at an altitude of 160 km.

With the aid of Figure 1-A-3 it is possible to estimate the magnitude of the positive going vehicle potential in the D-region under daytime conditions. This is done by equating $i_{pho}$ to $i_{am} \equiv 1/4\ N_e\ ev_e$, where $N_e$ and $v_e$ are respectively the density and thermal velocity of the ambient electrons. In a realistic situation equation (2, A-3) should be replaced by

$$\int_{S_{am}} i_{am}\, dS = \int_{S_{pho}} i_{pho}\, dS \qquad (3, A-3)$$

where the intergrations are performed over two unequal surface areas. For our purpose however we will ignore this factor and estimate only an upper limit to the positive vehicle potential. On the right hand vertical scale of Figure 1-A-3 is plotted the density of ambient electrons required to make $i_{am} = i_{pho}$, (here we have used the value $v_e = 9 \times 10^6$ cm/sec). Thus we see that at an altitude where $N_e = 10^3$ cm$^{-3}$ (i.e. typically 80 km) the vehicle potential will not be more positive than +2 eV.